

Contribution to the problem of near-zone inverse Doppler effect

Yehuda Ben-Shimol and Dan Censor

Department of Electrical and Computer Engineering, Ben-Gurion University of the Negev
Beer-Sheva, Israel

Abstract. The existence of an inverse Doppler effect in free space is again scrutinized, following some papers predicting the existence of such phenomena in the near zone of a moving oscillating three-dimensional dipole. In the present paper the wave scattered from a perfectly conducting thin cylinder moving in the presence of a plane electromagnetic wave is analyzed. The response of such a cylinder may be considered as due to either a two-dimensional monopole or a two-dimensional dipole in accordance with the polarization of the incident wave. An intensive numerical spectral estimation based on the fundamental definitions of the terms “frequency,” “spectrum,” and “uncertainty” is performed on the scattered wave at various ranges. An inverse Doppler effect was not found for the two-dimensional case. The same analysis was applied to the case of a moving three-dimensional radiating dipole, reconfirming previous results which showed the presence of an inverse Doppler effect in the near zone of the three-dimensional dipole.

1. Introduction

When an observer in free space is in motion relative to a monochromatic source, the frequency measured by him/her will be higher than the source-frequency (blue shift) when approaching the source and lower (red shift) when receding. This effect is known as the Doppler effect [Doppler, 1842] and has served as a major subject for researchers dealing with various applications of this phenomenon (see Gill [1965] for a good introduction to the Doppler effect). The term “inverse Doppler effect” is associated with the possibility that an approaching observer will recognize a red shift, and a receding one, a blue shift. Even if at a first glance such a phenomenon may sound unrealistic, some publications mention the possibility of an inverse Doppler effect in moving dispersive media (for example, unmagnetized cold plasma) [Frank, 1943; Papas, 1965; Rydbeck, 1960] where the inverse effect may occur under special circumstances. There are also other discus-

sions on inverse Doppler effect in free space [Engheta *et al.*, 1980; Engheta, 1990], which analyze the electromagnetic field of an oscillating three-dimensional (3-D) dipole in free space in the presence of a moving observer. However, these two cases are different, recasting their different spectral contents. In the case of dispersive media (e.g., unmagnetized cold plasma), the discussion may be restricted to a plane wave of certain frequency, and the Doppler effect is therefore evident. On the other hand, the components of the fields which are radiated from the oscillating 3-D dipole, as measured by a moving observer, may be represented in the form of time-varying amplitude $A(t)$ multiplied by an exponent of a time-varying phase $\phi(t)$, i.e.,

$$s(t) = A(t)e^{i\phi(t)} \quad (1)$$

In general, $s(t)$ cannot be represented by a single-frequency component, and one must consider the effect of the motion on both $A(t)$ and $\phi(t)$. Therefore the simple (and intuitive) definition for the Doppler effect as usually given for plane waves is no longer appropriate, and new definitions must be specified.

The spectral analysis of signals which are represented by (1) may be called “time-frequency analysis” and already constitutes a fundamental research

Copyright 1998 by the American Geophysical Union.

Paper number 98RS00033.
0048-6604/98/98RS-00033\$11.00

subject for many decades (see *Cohen* [1995] for a summary and references on this subject). The basic objective of such time-frequency analysis is to devise a function that will describe the energy density of a given signal in time and frequency. Analysis of the properties of such densities is based on analytic signals, which are in the form of (1), and their imaginary part is constructed from the Hilbert transform of the real part [*Papoulis*, 1977; *Vakman*, 1968]. The complex representation of signals and waves which is common in electromagnetic theory is constructed differently (i.e., quadrature representation) but may serve as a good approximation to the analytic representation for band-limited signals or, more generally, for signals when most of the spectrum resides in the positive side of the frequency axis.

The purpose of the present work is to study the phenomenon of the near-zone Doppler effect in free space on the basis of time-frequency analysis. The case of a radiating infinitesimal 3-D dipole has been investigated previously by *Engheta et al.* [1980] and *Engheta* [1990], who represented the analyzed wave in the form of (1) and defined the Doppler shift as the difference between the instantaneous frequency as measured by the moving observer and the intrinsic frequency of 3-D dipole oscillations. According to this definition, an inverse Doppler shift was found in the near zone of the 3-D dipole for some cases of observer motion.

Usually, the instantaneous frequency

$$\omega(t) \doteq \frac{d\phi(t)}{dt} \quad (2)$$

is used as a generalization of the term "frequency" in cases where the amplitude is constant or varies slowly, i.e., cases which match the common intuition. Analysis of more complicated cases must rely on energy distributions, and for most of them the envelope is concentrated in the vicinity of the instantaneous frequency. The instantaneous frequency is not a local parameter as one may deduce from (2); it is actually the average of all frequencies in a given time. Since the spread of the frequencies is determined by the behavior of the signal's amplitude, a measurement of this spread may be defined as

$$\sigma = \left| \frac{A'(t)}{A(t)} \right| \quad (3)$$

and 2σ is sometimes called the instantaneous bandwidth of the signal. The larger the instantaneous bandwidth gets, the wider the spread of the frequen-

cies is, and the mean frequency (i.e., instantaneous frequency) no longer serves as a good measure for the signal's frequency.

Common to all situations of "head-on" observer motion is a "collision" between the observer and the dipole, i.e., overlapping of position, thus generating infinite field values. Furthermore, the analysis given by *Engheta et al.* [1980] and *Engheta* [1990] did not consider the properties of the amplitude which vary rapidly in the near zone of the dipole. The effects of such amplitude changes on the spectrum (or energy density) do not appear in the instantaneous frequency, which is computed from the phase alone.

In order to enhance the analysis, the effect of amplitude changes must be considered too; thus parameters such as the instantaneous frequency must be examined carefully with regard to the signal's bandwidth 2σ , as done in the present work.

In addition to the "instantaneous methods" it was decided in the present work to examine the Doppler effect in the far and near zone of the radiating dipole on the basis of short-time Fourier spectral analysis. The spectrogram method (which is based on short-time Fourier analysis) uses both amplitude and phase in the calculation, thus preventing potentially erroneous interpretations which are based on the phase only.

The phenomenon of inverse Doppler effect in the near zone of the 3-D elementary dipole is somewhat unrealistic, because the effects of the system exciting the dipole and the associated circuitry are ignored. This motivates the investigation of the near-zone Doppler effect of scattering by two-dimensional (2-D) monopole and dipole where the excitation is external, for example, an incident plane wave. Accordingly, the oscillating 3-D dipole discussed by *Engheta et al.* [1980] was replaced by a perfectly conducting, thin cylinder moving in free space in the presence of an exciting plane wave. The response of the cylinder may be taken to be due to a 2-D monopole or a 2-D dipole (in addition to a 2-D monopole term) for electric or magnetic polarization of the incident plane wave, respectively. *Van Bladel* [1985] give a good summary of the spectral properties of the reflected wave in the far zone. *Michielsen et al.* [1981] and *de Zutter* [1982, 1987] provide general analytical calculation of the Fourier spectra of the scattered wave (for 3-D cases also).

A fixed observer positioned at the origin of the laboratory frame of reference measures the scattered wave which contains information on the motion of the

scatterer. The observer's position was slightly displaced, to prevent a collision with the moving cylinder, and thus the amplitudes of the electromagnetic fields remain finite. However, the smaller the offset a gets (see Figure 6), the higher the value of the fields are in the near zone.

While performing a spectral analysis, the principle of uncertainty should be borne in mind; that is, when dealing with real situations, signals of infinite time duration are not available, and the spectral analysis turns to spectral estimation. We use the term "uncertainty" in the context of signal analysis, which should not be confused with the principle of uncertainty of quantum mechanics. The Fourier transform $S(\omega)$ of the deterministic time signal $s(t)$ is given by

$$S(\omega) = \int_{-\infty}^{\infty} s(t)e^{-i\omega t} dt \quad (4)$$

and the power spectrum $P_s(\omega)$ is defined by

$$P_s(\omega) = |S(\omega)|^2 \quad (5)$$

and involves values of $s(t)$ of all times. If $s(t)$ represents the measured signal, its exact spectral content is given by (5) without us being able to associate each spectral component with its range in space (i.e., we have here a complete uncertainty of range), so the spectral contents of the near and far zones from both approaching and receding scatterers would be inseparable. In order to increase range accuracy, the measured signal is sliced to overlapping segments, and a spectral analysis is performed separately on each segment, using the short-time Fourier transform

$$S_T(\omega) = \int_{t_0}^{t_0+T} s(t)e^{-i\omega(t-t_0)} dt \quad (6)$$

The finite duration of the segmented signal, T , broadens the spectrum, and this broadening is increased as the duration of the segment diminishes. The implication of such broadening is an increase in the uncertainty of the spectral components [Papoulis, 1977; Vakman, 1968]. It is interesting to note that the uncertainty principle applies also to the measurement of the instantaneous frequency [Papoulis, 1977; Vakman, 1968]. In the present case, there is no unique way of defining the optimal time segment width, and hence a variety of width values was tested during the simulation in order to detect an inverse Doppler effect in the near zone of the moving scat-

terer. An inverse Doppler effect has not been detected in the near zone of the moving cylinder.

2. The Three-Dimensional Dipole

In this section we will describe succinctly the analysis reported by *Engheta et al.* [1980] and *Engheta* [1990]. Only the parts which are most essential to the discussion of this paper are included. Figure 1 describes the analyzed configuration, in which an infinitesimal, oscillating electric dipole is positioned at the origin of the laboratory frame of reference and lying along the z axis. An observer is moving with constant velocity in free space and measures the electromagnetic fields which are radiated by the dipole for few cases of motion direction. Let us denote the laboratory frame of reference by Γ and the frame of reference comoving with the observer by Γ' . The electromagnetic fields of the oscillating electric dipole in Γ are given by equations (1) and (2) of *Engheta et al.*[1980]. (Note that there are some typographical errors in *Engheta*[1990].)

In the first case, which *Engheta et al.* [1980] and *Engheta* [1990] analyzed, the observer moves on the equatorial plane of the dipole, along the y axis from $y = -\infty$ to $y = \infty$ with constant velocity $\mathbf{v} = v\hat{\mathbf{y}}$. It is evident that the observer approaches the dipole for $t' < 0$ and recedes from the dipole for $t' > 0$. Using the transformations of special relativity, we get

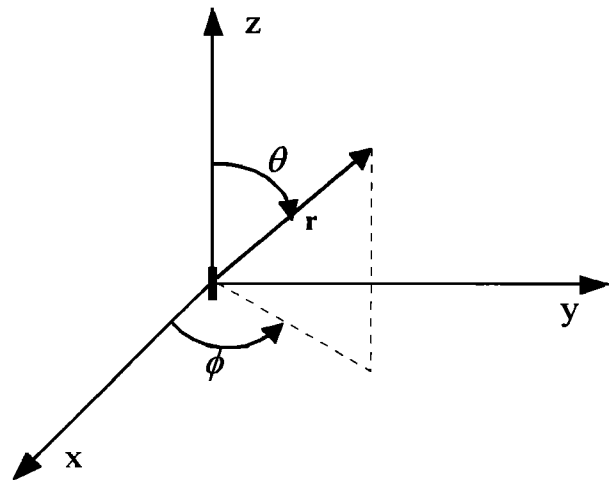


Figure 1. An infinitesimal oscillating electric dipole positioned at the origin of the laboratory frame of reference.

$$E'_{\theta'} = \begin{cases} -\frac{p}{4\pi\epsilon_0 vt'} \left[\frac{ik}{vt'} - \frac{1}{(vt')^2} + k^2 + ik\beta \left(ik - \frac{1}{vt'} \right) \right] \exp[i(kv - \omega)t'] & t' > 0 \\ -\frac{p}{4\pi\epsilon_0 vt'} \left[\frac{ik}{vt'} + \frac{1}{(vt')^2} - k^2 + ik\beta \left(ik + \frac{1}{vt'} \right) \right] \exp[-i(kv + \omega)t'] & t' < 0 \end{cases} \quad (7)$$

and

$$H'_{\phi'} = \begin{cases} \frac{p}{4\pi vt'} \left[i\omega \left(ik - \frac{1}{vt'} \right) + v \left(\frac{ik}{vt'} - \frac{1}{(vt')^2} + k^2 \right) \right] \exp[i(kv - \omega)t'] & t' > 0 \\ \frac{p}{4\pi vt'} \left[-i\omega \left(ik + \frac{1}{vt'} \right) - v \left(\frac{ik}{vt'} + \frac{1}{(vt')^2} - k^2 \right) \right] \exp[-i(kv + \omega)t'] & t' < 0 \end{cases} \quad (8)$$

where p is the electric dipole moment, ϵ_0 is the permittivity of free space, $k = \omega/c$, and c is the speed of light in free space.

In order to represent the electromagnetic fields in Γ' in the form of (1) (which is actually a quadrature representation), one may write

$$\begin{aligned} E'_{\theta'} &= |E'_{\theta'}| \exp(i\psi'_{e'\theta'}) \exp(-i\omega t') \\ H'_{\phi'} &= |H'_{\phi'}| \exp(i\psi'_{m'\phi'}) \exp(-i\omega t') \end{aligned} \quad (9)$$

The motion affects the amplitudes $|E'_{\theta'}|$, $|H'_{\phi'}|$ and the phases $\psi'_{e'\theta'}$, $\psi'_{m'\phi'}$, which may be measured by the observer in Γ' . Neglecting the effect of the motion on the amplitudes (and the spectrum) *Engheta et al.* [1980] used the time derivative of the phases $\psi'_{e'\theta'}$ and $\psi'_{m'\phi'}$ for the electric and magnetic fields of the 3-D dipole, respectively.

The instantaneous frequency in Γ' frame for low velocities (i.e., $\gamma \cong 1$) is given by

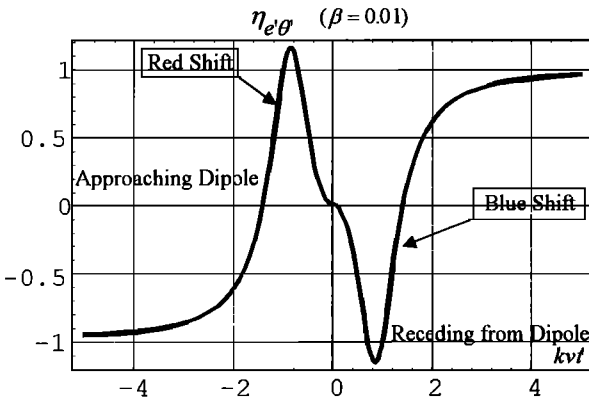


Figure 2. Normalized Doppler shift $\eta_{e'\theta'}$ for $E'_{\theta'}$ in the equatorial plane of the dipole. Positive and negative values correspond to red and blue Doppler shifts, respectively. (Recomputed after *Engheta* [1990]).

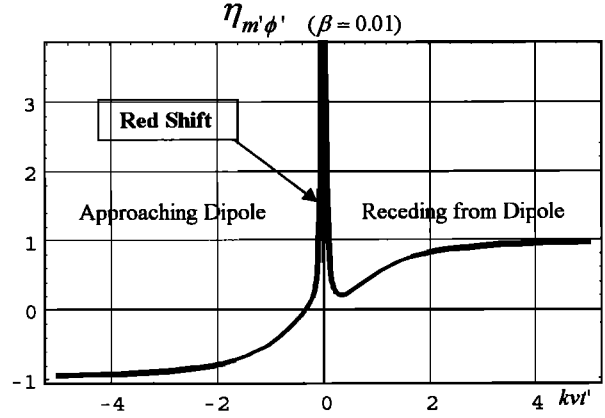


Figure 3. Normalized Doppler shift $\eta_{m'\phi'}$ for $H'_{\phi'}$ in the equatorial plane of the dipole. Positive and negative values correspond to red and blue Doppler shifts, respectively. (Recomputed after *Engheta* [1990]).

$$\omega' = \omega [1 - \beta\eta] \quad (10)$$

where

$$\eta = \frac{1}{kv} \frac{d\psi'}{dt'} \quad (11)$$

and the notations $\psi'_{e'\theta'}$, $\psi'_{m'\phi'}$ are used for the electric and magnetic fields, respectively. Similar notation is used later for η . From (10) it is understood that η represents the normalized difference in the instantaneous frequencies between Γ and Γ' frames and is given by

$$\eta_{e'\theta'} = \begin{cases} \frac{[(kvt')^2(1-\beta)-1]^2 - (1-\beta)}{[(kvt')^2(1-\beta)-1]^2 + [kvt'(1-\beta)]^2} & t' > 0 \\ -\frac{[(kvt')^2(1+\beta)-1]^2 - (1+\beta)}{[(kvt')^2(1+\beta)-1]^2 + [kvt'(1+\beta)]^2} & t' < 0 \end{cases} \quad (12)$$

for the electric field and

$$\eta_{m'\phi'} = \begin{cases} \frac{[(kvt')^2(1-\beta)+\beta]^2 - \beta(1-\beta)}{[(kvt')^2(1-\beta)+\beta]^2 + [kvt'(1-\beta)]^2} & t' > 0 \\ -\frac{[(kvt')^2(1+\beta)-\beta]^2 - \beta(1+\beta)}{[(kvt')^2(1+\beta)-\beta]^2 + [kvt'(1+\beta)]^2} & t' < 0 \end{cases} \quad (13)$$

Plots of $\eta_{e'\theta'}$ and $\eta_{m'\phi'}$ are given in Figures 2 and 3, respectively, showing an inverse Doppler effect in the near zone of the dipole, according to the definitions given in (11) and (10).

The above difficulties, which arise from the definition of the instantaneous frequency, may lead us to erroneous physical interpretations of the analyzed phenomenon (i.e., the Doppler shift in the present case). If a phenomenon such as illustrated by the example, which is described in the appendix, does exist

in the present case, the determination of the inverse Doppler effect may be incorrect.

In spite of the mentioned difficulties, in many cases the instantaneous frequency is considered as an instantaneous parameter, i.e., the frequency of the signal at a given time t is determined locally with no concern to the signal's properties in the past or the future. However, the definition of the instantaneous frequency is associated with analytic signals, which, in turn, are calculated by using the signal values for all times. Actually, the instantaneous frequency is the average frequency at a given time [Cohen, 1995], and the spread of signal's energy around this average frequency (i.e., instantaneous bandwidth) will determine whether the use of the average is appropriate in the case at hand. In other words, one must consider the effect of the motion on the amplitude. The ratio between the instantaneous frequency and the instantaneous bandwidth may be called an "instantaneous quality factor" (similar to the definition of the quality factor in filter theory) Q , i.e.,

$$Q = \frac{\omega'}{2\sigma'} \tag{14}$$

Using (7) and (8), the normalized instantaneous bandwidth (2σ) is given by

$$\sigma'_e = \frac{\frac{1}{kv} \left| \frac{d|E'_{\theta'}|}{dt'} \right|}{|E'_{\theta'}|} = \begin{cases} -\frac{1}{(kvt')} \frac{[(kvt')^2(1+\beta)-1]^2 + 2[(kvt')^2\beta(1+\beta)+1]}{[(kvt')^2(1+\beta)-1]^2 + [(kvt')(1+\beta)]^2} & \text{for } t' < 0 \\ \frac{1}{(kvt')} \frac{[(kvt')^2(1-\beta)-1]^2 + 2[(kvt')^2\beta(1-\beta)+1]}{[(kvt')^2(1-\beta)-1]^2 + [(kvt')(1-\beta)]^2} & \text{for } t' > 0 \end{cases} \tag{15}$$

for the electric field and

$$\sigma'_m = \frac{\frac{1}{kv} \left| \frac{d|H'_{\phi'}|}{dt'} \right|}{|H'_{\phi'}|} = \begin{cases} -\frac{1}{(kvt')} \frac{((1+\beta)(kvt')^2 - \beta)^2 + 2\beta[(1-\beta)(kvt')^2 + \beta]}{(kvt')[(1+\beta)(kvt')^2 - \beta]^2 + [(kvt')(1+\beta)]^2} & \text{for } t' < 0 \\ \frac{1}{(kvt')} \frac{[(kvt')^2(1-\beta) - \beta]^2 + 2\beta[(kvt')^2(1-\beta) + \beta]}{[(1-\beta)(kvt')^2 - \beta]^2 + [(kvt')(1-\beta)]^2} & \text{for } t' > 0 \end{cases} \tag{16}$$



Figure 4. Instantaneous quality factor Q for the electric field of the three-dimensional (3-D) dipole. The inverse effect resides between each pair of bold points and is accepted only for large Q values.

for the magnetic field. Large Q factors (i.e., $Q \gg 1$) indicate narrow bandwidth, and the use of instantaneous frequency as the dominant frequency in Γ' frame is valid. In contrast, small Q values (i.e., $Q \ll 1$) indicate that the bandwidth is wide and the instantaneous frequency cannot represent the measured signal as a dominant frequency. Figures 4 and 5 show the behavior of Q versus $kv t'$ for different values of the observer's velocity. It seems that for the electric field, the use of the instantaneous frequency is valid for most of the range, showing that an inverse effect does exist. As for the magnetic field, the inverse effect which was reported by *Enggheta et al.* [1980] and *Enggheta* [1990], happens very near to the dipole's location where Q values are relatively small, or, in other words, the inverse effect is acceptable only for very small β values (i.e., $\beta < 0.01$).

In many cases (i.e., for signals of relatively large Q factors) the instantaneous frequency coincides with the location of the maximum of the distribution versus time, and therefore if one determines the frequency of the signal as the frequency where the maximal power spectrum (or distribution) occurs, the results will likely be identical. Another fact which must be remembered is that in reality the observer may only measure real signals which do not come in the form $A(t) \cos \phi(t)$. Therefore, in order to calculate the dominant frequency, one must calculate an analytic complex signal (by using the Hilbert transform of the real part as the imaginary part of the complex signal) from which the phase may be determined or, alternatively, use spectral techniques.

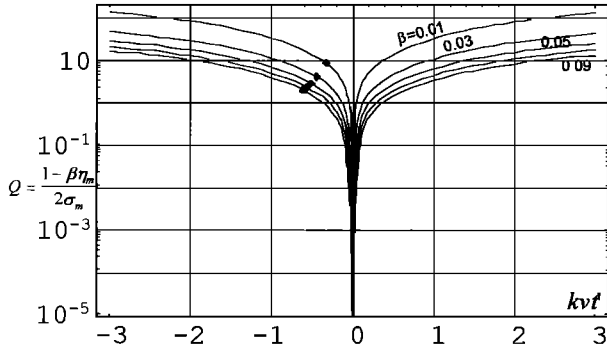


Figure 5. Instantaneous quality factor Q for the magnetic field of the 3-D dipole. The inverse effect resides between the bold point and the vertical axis and is accepted only for large Q values.

3. The Two-Dimensional Case: The Moving Cylinder

The inverse Doppler effect which takes place in the near zone of the 3-D radiating dipole raises the question whether such a phenomenon also occurs for other type of radiators or scatterers in free space. The following description and analysis covers the two-dimensional case.

Figure 6 describes the configuration of the following theoretical experiment: A circular cylinder with constitutive parameters μ_i, ϵ_i , moves with constant velocity \mathbf{v} in the presence of a plane electromagnetic wave in free space (ϵ_0, μ_0). Here we denote the frame of reference comoving with the cylinder by Γ_1 in order to avoid confusion between “primed” physical quantities (that is, measured in the comoving frame of reference) and the derivatives of other physical quantities which appear later in the laboratory frame

of reference. The incident plane wave may be electrically polarized or magnetically polarized parallel to the cylinder’s axis. A fixed observer, positioned at the origin of the laboratory frame of reference Γ_0 , measures the wave scattered by the cylinder. This scattered wave is analyzed in order to determine the Doppler effect as a function of time (i.e., as a function of the instantaneous cylinder’s position in Γ_0).

The calculation of the scattered wave is based on the transformations of special relativity. In Figure 6 the y axes of Γ_0 and Γ_1 coincide at $t_1 = t_0 = 0$; and a is the minimal distance between the observer and the cylinder axis. The incident wave \mathbf{U}_{inc0} is plane and may be written in Γ_0 as

$$\mathbf{U}_{inc0} = \mathbf{f}_0 e^{i\mathbf{k}_0 \cdot \mathbf{r}_0 - i\omega_0 t_0} \tag{17}$$

where \mathbf{f}_0 defines the polarization of the incident wave and has a magnitude of one, \mathbf{k}_0 defines the direction of propagation, and ω_0 is the angular frequency.

The resulting scattered wave measured by an observer in Γ_0 when expressed in terms of Γ_0 is a complicated expression involving Γ_0 time and space coordinates \mathbf{r}_0, t_0 , in mixed form. The representation is simpler in form when the scattered wave in Γ_0 is expressed in terms of time and space coordinates \mathbf{r}_1, t_1 , of Γ_1 [Censor, 1967, 1969, 1972]

$$U_0^{(1)}(\mathbf{r}_1, t_1) = \gamma f_1 e^{-i\omega_1 t_1} \sum i^n b_n(\alpha_1, \beta) H_n(k_1 r_1) e^{in\theta_1} \tag{18}$$

where the scattering coefficients in Γ_0 are

$$b_n(\alpha_1, \beta) = a_n(\alpha_1) + \frac{\beta}{2} [a_{n-1}(\alpha_1) + a_{n+1}(\alpha_1)] \tag{19}$$

and $a_n(\alpha_1)$ may be approximated by

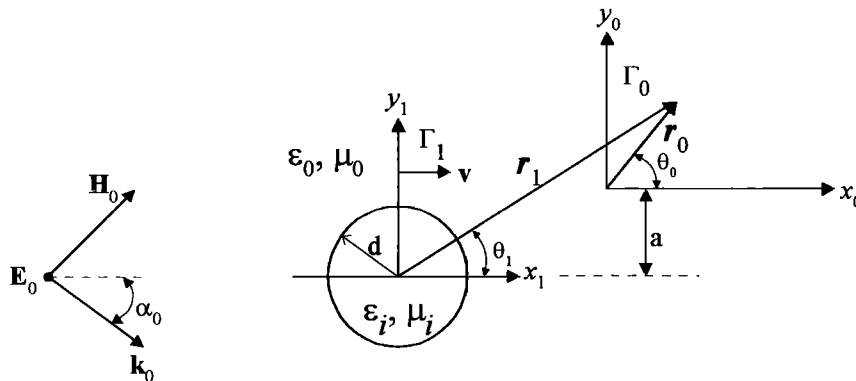


Figure 6. A moving cylinder in the presence of an incident plane wave.

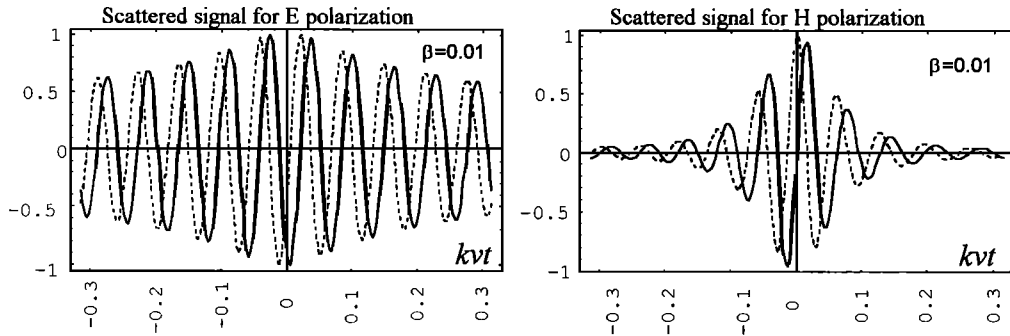


Figure 7. The wave scattered from a thin cylinder as measured by an observer in the laboratory frame of reference. The imaginary part is represented by a dashed line.

$$\begin{aligned}
 a_0 &\approx -\frac{i\pi}{2\ln(2/\delta k_1 d)} & \delta &= 1.781\dots \\
 a_n(\alpha_1) &\approx -e^{-in\alpha_1} i n \pi \frac{(k_1 d/2)^{2n}}{(n!)^2} & n &= 1, 2, 3, \dots
 \end{aligned}
 \tag{20}$$

for electrical polarization and

$$\begin{aligned}
 a_0 &\approx -i\pi (k_1 d/2)^2 \\
 a_n(\alpha_1) &\approx e^{-in\alpha_1} i n \pi \frac{(k_1 d/2)^{2n}}{(n!)^2} & n &= 1, 2, 3, \dots
 \end{aligned}
 \tag{21}$$

for magnetic polarization. For electrical polarization the monopole term a_0 is dominant, as seen in (20). For magnetic polarization, a_0 and a_1 are of the same order, and thus the monopole and dipole terms are dominant, as can be seen from (21). Here α_0, α_1 are the angles subtended by the propagation vectors $\mathbf{k}_0, \mathbf{k}_1$, respectively, and the velocity \mathbf{v} in Γ_0, Γ_1 , respectively, as described in Figure 6.

In the present paper, a symmetrical Doppler effect in the far zones was chosen, prescribing that the incident wave propagates in a direction perpendicular to the velocity (i.e., $\mathbf{k} \cdot \mathbf{v} = 0$). Therefore $\alpha_0 = \pi/2$. Hence, for the incident wave, a transverse Doppler effect is discussed. For $\alpha_0 = \pi/2$, the scattered wave, for both electric and magnetic polarization, is illustrated in Figure 7.

4. Spectral Analysis of the Doppler Effect

The relativistic Doppler effect, as stated in the beginning of this paper, is derived from the Lorentz transformations when the electromagnetic fields are plane waves. In this case the effect of the motion on

the frequency may be separated from the effect on the amplitude, since the transformed waves remain plane. For nonplanar waves, the given definition of Doppler effect is still useful if the given nonplanar wave is recast as a superposition (integral) of plane waves [Censor, 1991; Stratton, 1941]. The transformation of such nonplanar waves from one inertial frame to another may be derived by direct transformation of each component plane wave included in the given nonplanar wave spectral representation. In the present case the scattered wave in Γ_1 and in Γ_0 are not planar, as may be seen from (18), and the effect of the motion on the phase cannot be separated from the effect of the motion on the time-dependent amplitude.

The presence of a frequency component (i.e., a sine wave of a given frequency) in a given time signal is identified by a high peak in its power spectrum (equation (5)) at that frequency. This property will serve to identify the dominant frequency component of the scattered wave. Since an analytic expression of the short-time Fourier transform (6) of the scattered wave (18) is not available, the power spectral density must be estimated with a numerical spectral estimator. Spectral estimators may be divided into two main categories: (1) nonparametric (or classical) spectral estimators which are based on the discrete Fourier transform algorithm (DFT) and (2) parametric (or modern) spectral estimators which are based on some models describing the behavior of the analyzed signal or its spectrum.

In the present simulation it was decided to use a DFT based algorithm and its efficient implementation, the fast Fourier transform (FFT) algorithm [Cooley and Tukey, 1965; Ifeachor and Jarvis, 1993;

Kay, 1988; *Marple*, 1987]. An extensive discussion of spectral analysis and estimation is given by *Kay* [1988] and *Marple* [1987].

The use of a numerical computation forces us to set specific values for each parameter which takes part in the analyzed configuration. The cylinder motion has been simulated so that the cylinder traverses a trajectory parallel to the x axis from large negative x values to large positive x values moving with constant velocity. The cylinder is located below the x axis of the laboratory frame of reference Γ_0 (see Figure 6) so it does not coincide (i.e., collide) with the observer, and infinite field values are thus avoided. The incident plane wave is chosen at 1 GHz frequency, and the velocity of the cylinder is much lower than the speed of light, although the relativistic formalism is retained for all cases (various cases were tested by us, but only a few results are presented in the figures given here). Consequently, the Doppler frequency shift in the far zone is much lower than the carrier frequency, and thus the resolution capability of the spectral estimator must be considered in order to get results with sufficient accuracy. For the chosen velocity, say 3×10^6 m/s (i.e., $\beta = 0.01$), the Doppler shift in the far zone is of the order of megahertz, and may be even less in the near zone. For carrier frequency in the RF range (1 GHz in the present example), a vast number of samples (2×10^8 samples for a resolution of 10 Hz with a sampling frequency of 2 GHz) has to be included in each analysis in order to detect the frequency change with sufficient accuracy, thus rendering such computations impractical. Fewer sam-

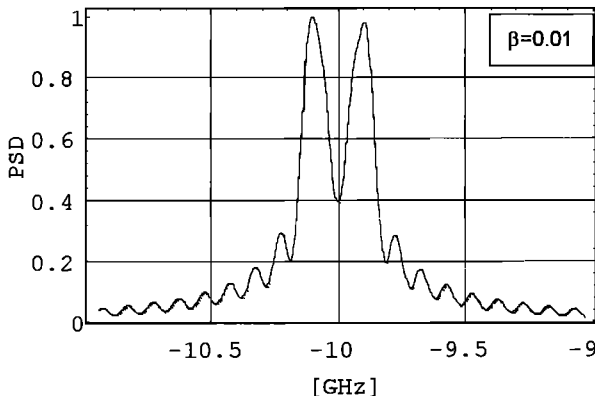


Figure 8. Normalized power spectral density (PSD) of the wave scattered from a moving monopole (E polarization). The time signal covers the near and far zones.

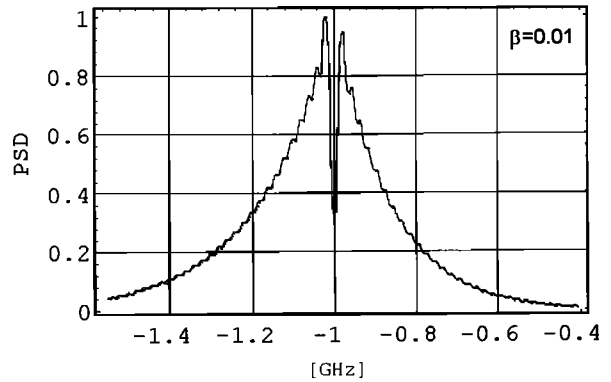


Figure 9. Normalized PSD of the wave scattered from a moving dipole (H polarization). The time signal covers the near and far zones.

ples cause poorer frequency resolution. The FFT algorithm is designed for optimal DFT computation, i.e., for N discrete frequency values. In order to make such computations practical, the location of the peak of the power spectrum is obtained in two steps. An initial estimation of the peak location is computed with a short FFT algorithm (i.e., low number of discrete frequency values). This initial estimation is used later to define the limits where this peak occurs solely (i.e., without sidelobes). Later, an optimization algorithm searches for the location of the peak using the DTFT (discrete time Fourier transform) algorithm (i.e., the frequency values are continuous). The use of the initial FFT estimation prevents the detection of sidelobes and reduces the number of DFT computations which are needed for the required frequency resolution (1 Hz in the present paper).

As mentioned earlier, there has to be some balance between the requirements of an exact frequency determination (i.e., analysis of long signal duration) and the determination of the exact time when this frequency occurs (i.e., analysis of short signal duration). In the extreme case where the signal from all ranges is used to calculate the spectrum, the power spectral density (PSD) contains two large peaks at frequencies belonging to the far zones (and which are predicted by the relativistic transformations for plane waves), but there is no way to determine when these frequencies appear in the original signal (see Figures 8 and 9 for electric and magnetic polarization, respectively). Furthermore, the analyzed signal contains information from the far and near zones

which cannot be resolved from the power spectrum. In order to decrease time uncertainty and enable a spectral analysis at “specific locations” of the cylinder, a sliding rectangular time window was introduced, i.e., the scattered wave was divided into overlapping segments. For each such segment the PSD is calculated using samples from that segment, and the frequency in which the maximal power value appeared was taken to be the Doppler shift belonging to the center of the current segment. The window size (i.e., the time extent of each segment) has been varied from small values covering about one cycle of the measured signal in the far zone to the extreme case where a single window covered almost the full signal, in order to get the optimal window which yields the best frequency-location information.

Summarizing the description above, the numerical simulation and analysis is composed of the following steps:

1. The scattered wave, as measured by the observer at the origin of Γ_0 , is simulated using equation (18) and the scattering coefficients given in equations (20), (21) (for electric and magnetic polarization, respectively), and (19). The time range covers the near and far zones of the observer. Examples of such signals are shown in Figure 7 for both electric and magnetic polarization.
2. The scattered wave is divided into overlapping segments, and each is zero padded and processed by an FFT algorithm. From the FFT transform a power spectrum is calculated. The initial estimation of the

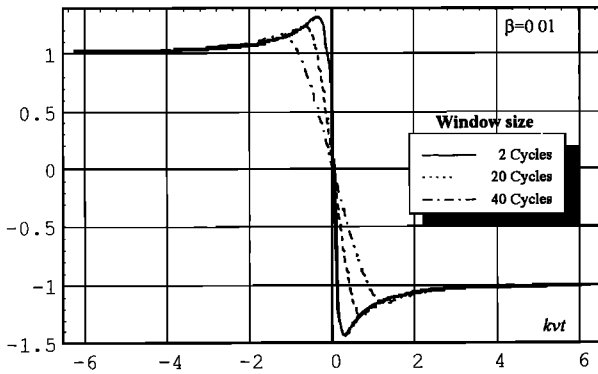


Figure 10. Normalized Doppler shift for the moving 2-D monopole. The discrete Fourier transform (DFT) based algorithm is used for the computations. In general, narrow windows follow better rapid amplitude changes in the near zone.

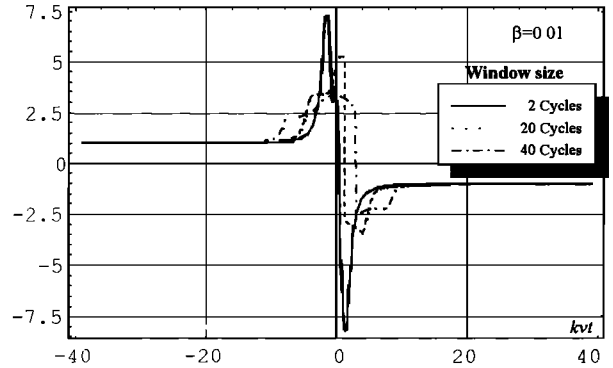


Figure 11. Normalized Doppler shift for the moving 2-D dipole. The incident wave is magnetically polarized, and the DFT-based algorithm is used for the computations. Each line represents a different different window width which is measured in numbers of cycles of the measured signal in the far zone (solid line, two cycles; dashed line, 20 cycles; dash-dotted line, 40 cycles). In general, narrow windows follow better rapid amplitude changes in the near zone.

Doppler shift is defined as the frequency in which the maximal value of the power spectrum occurs.

3. A more accurate computation of the Doppler frequency (using the above definition) is obtained by an optimization algorithm. The algorithm is based on a minimum finding algorithm around the Doppler frequency which is determined by the previous step.

4. The frequency of the peak is assigned to the center of the time segment

5. Discussion

Some results of the computed Doppler shift are presented in Figures 10 and 11 for a moving 2-D monopole and a moving 2-D dipole, respectively. In the far zone, the computed Doppler shift fits the theoretical value which may be obtained analytically by substituting the asymptotic expression of Hankel function for large arguments in (18). In the near zone, the transition from the $t_0 < 0$ range (cylinder approaching) to the $t_0 > 0$ range (cylinder receding) is not abrupt; that is, the Doppler frequency shift changes gradually, but the change is not monotonic. The fast change of the amplitudes of the scattered waves in the near zone of the cylinder is shown in Figure 7 and appears as a high frequency-component in the PSD. This may explain the difference between Figure 10 (monopole) and Figure 11 (dipole). The

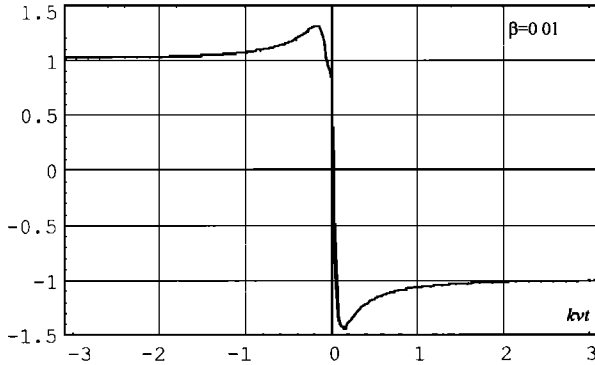


Figure 12. Normalized Doppler shift (relative to $\omega\beta$) versus kvt for the moving 2-D monopole. The instantaneous frequency is computed numerically. The increase in frequency in the near zone follows the fast amplitude change.

relative amplitude change for the dipole case is faster than in the monopole case which is supported by the results shown in Figures 10 and 11, i.e., the increase of the Doppler shift in the near zone of the cylinder. Close examination of Figures 10 and 11 shows that near the origin, for $0 < kvt \ll 1$, the Doppler shift is still positive. This should not be interpreted as an inverse Doppler effect since it is caused by the finite width of the slicing window. As the width of the slicing window increases, more information from the past (relative to the window's midpoint) is involved with the computation, thus slowing the response to the change in the Doppler shift at positive times.

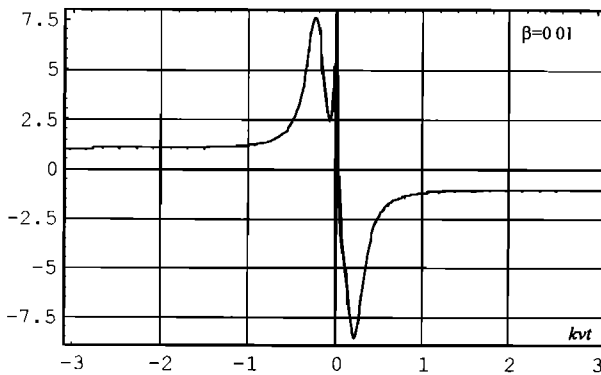


Figure 13. Normalized Doppler shift (relative to $\omega\beta$) versus kvt for the moving 2-D dipole. The instantaneous frequency is computed numerically. The increase in frequency in the near zone follows the fast amplitude change.

The effect is more pronounced for the 2-D dipole case (i.e., magnetic polarization). In addition, a numerical computation of the instantaneous frequency for the 2-D case is presented in Figures 12 and 13. The results agree with Figures 10 and 11. The numerical computation of the instantaneous frequency is much faster and more efficient than the DFT-based algorithm but is more sensitive to the presence of noise, which usually occurs in real situations. Moreover, the computations of differences as an approximation to the analytical derivatives may be inaccurate for fast changes (which appear in the near zone), and one has to sample the signal with a very high sampling frequency, which may lead to other numerical problems such as accuracy and round-off errors.

Various sets of simulation parameters such as cylinder velocity, segment width, sampling frequency, etc., were used in order to discover an inverse Doppler shift in the near zone of the 2-D cylinder. Such an effect was not found.

The DFT-based algorithm was applied to the measured fields of the 3-D moving dipole. Since a singularity occurs in (7) and (8) for $t' = 0$, the trajectory of the moving observer was slightly displaced above the y axis and parallel to it, so collision was avoided. The results are given in Figures 14 and 15 and are in agreement with the results given by *Engheta et al.* [1980] and *Engheta* [1990], except for a very narrow region near the origin, where the rapid change of signal values is characterized by very high frequencies where the peaks of the PSDs occur and are selected as the dominant frequencies.

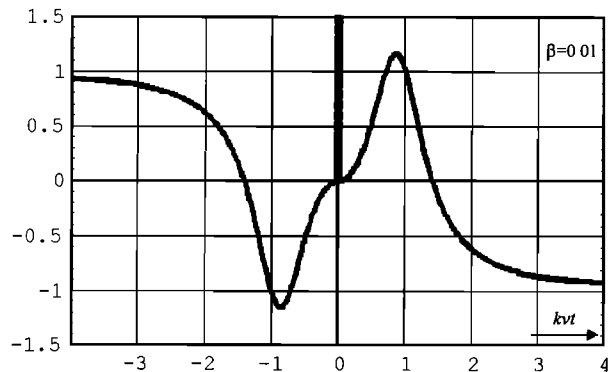


Figure 14. Normalized Doppler shift (relative to $\omega\beta$) computed with the DFT-based algorithm. The inverse Doppler shift appears in the near zone. Close to the origin, the effect of the fast amplitude change is dominant. The extent of the high frequency lags in proportion to the width of the slicing window.

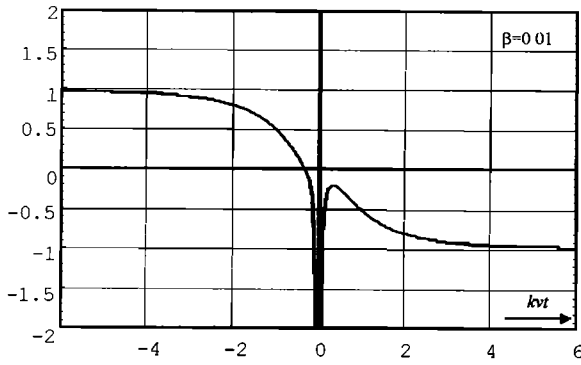


Figure 15. Normalized Doppler shift (relative to $\omega\beta$) for the magnetic field of the 3-D dipole as computed with the DFT-based algorithm. The inverse Doppler shift which appears in the near zone is very close to the origin, and thus may be invalid. Close to the origin, the effect of the fast amplitude change is dominant. The extent of the high frequency lags in proportion to the width of the slicing window.

6. Summary

The existence of the inverse Doppler effect in free space has been scrutinized, in view of some papers reporting the effect in the vicinity of a moving radiating 3-D dipole. The difference between the terms “frequency” and “instantaneous frequency” and their relation to the physical meaning of the Doppler effect were carefully considered. A theoretical experiment consisting of a moving perfectly conducting thin cylinder in the presence of an exciting plane wave was discussed. The response of the cylinder may be taken to be due to a 2-D monopole or a 2-D dipole for electric or magnetic polarization of the incident plane wave, respectively, therefore enabling us to compare our results with those of the 3-D case which were reported by *Engheta et al.* [1980]. The spectral analysis is based on the discrete time Fourier transform (DTFT) and its fast implementation (FFT). The measured signal was divided into overlapping segments in order to reduce the time uncertainty of the Doppler shift. A classical spectral estimator was applied to each such segment, and the Doppler shift was defined as the difference between the location of the highest peak of the PSD and the frequency of the exciting plane wave. The time instance of this Doppler shift was set at the center of the time segment. Intensive numerical analysis involving various sets of simulation parameters was

applied, and none of them show the existence of an inverse Doppler effect for the 2-D case.

For the three dimensional case, the analysis and results which were given by *Engheta et al.* [1980] and *Engheta* [1990] are rechecked with respect to the instantaneous bandwidth in the near zone. This examination supports the phenomenon of the inverse Doppler effect for the three-dimensional dipole in free space, excluding a very narrow zone where the fast change in the amplitude is not reflected in the instantaneous frequency. Analyzing the fields of the three-dimensional dipole with the DFT-based algorithm supports the existence of the inverse Doppler effect phenomenon and shows that in a very narrow region the fast change of the amplitude is dominant.

Appendix: A Simple Example

The behavior of “instantaneous frequency” (i.e., the time derivative of the phase) does not always serve as a generalization of the term “frequency,” as illustrated by the following example [after *Cohen*, 1995]: Take a time signal

$$\begin{aligned} f(t) &= s_1(t) + s_2(t) \\ &= A_1 e^{i\omega_1 t} + A_2 e^{i\omega_2 t} \\ &= A(t) e^{j\varphi(t)} \end{aligned} \quad (\text{A1})$$

where the amplitudes A_1 , A_2 are taken to be real constants and ω_1 , ω_2 are positive angular frequencies. Since ω_1 , ω_2 are taken to be positive, $s(t)$ is analytic. The power spectrum of $s(t)$ consists of two delta functions at (angular) frequencies ω_1 and ω_2 , i.e.,

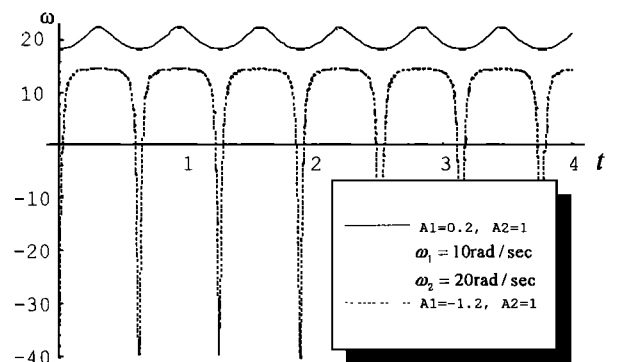


Figure 16. The instantaneous frequency of $A_1 e^{i\omega_1 t} + A_2 e^{i\omega_2 t}$. The dashed lines shows the possibility of negative frequency values for an analytic signal.

$$S(\omega) = A_1\delta(\omega - \omega_1) + A_2\delta(\omega - \omega_2) \quad (\text{A2})$$

The amplitude $A(t)$ and the phase $\varphi(t)$ are given by

$$A(t) = \sqrt{A_1^2 + A_2^2 + 2A_1A_2 \cos(\omega_1 - \omega_2)t} \quad (\text{A3})$$

and

$$\varphi(t) = \arctan \left(\frac{A_1 \sin \omega_1 t + A_2 \sin \omega_2 t}{A_1 \cos \omega_1 t + A_2 \cos \omega_2 t} \right) \quad (\text{A4})$$

respectively. The instantaneous frequency is calculated as the time derivative of the phase, i.e.,

$$\omega(t) = \frac{d\varphi(t)}{dt} = \frac{1}{2}(\omega_1 + \omega_2) + \frac{1}{2}(\omega_1 - \omega_2) \frac{A_2^2 - A_1^2}{A^2(t)} \quad (\text{A5})$$

Figure 16 illustrate the instantaneous frequency of the signal $s(t)$ for two cases. The following simple example illustrates some difficulties arising from the definition of the instantaneous frequency:

1. The instantaneous frequency is not necessarily one of the distinct frequencies in the spectrum (put $A_1 = A_2$ in (A5), for example).

2. The instantaneous frequency may be continuous, ranging over an infinite number of values even for a signal having a spectrum consisting of few distinct frequencies.

3. The instantaneous frequency may be negative for analytic signals (i.e. signals with zero spectrum for negative frequencies).

4. For band-limited signals the instantaneous frequency may extend outside the band.

References

- Censor, D., Scattering in velocity dependent systems (in Hebrew), D.Sci. thesis, Technion-Isr. Inst. of Technol., Haifa, Isr., 1967.
- Censor, D., Scattering of a plane wave at a plane interface separating two moving media, *Radio Sci.*, 4, 1079-1088, 1969.
- Censor, D., Scattering in velocity dependent systems, *Radio Sci.*, 7, 331-337, 1972.
- Censor, D., Application-oriented relativistic electrodynamics, in *Progress in Electromagnetics Research*, edited by J. A. Kong, chap.4, pp. 119-158, Elsevier, New York, 1991.
- Cohen L., *Time-Frequency Analysis*, Prentice-Hall, Englewood Cliffs, N. J., 1995.
- Cooley, J. W., and J. W. Tukey, An algorithm for the machine computation of complex Fourier series, *Math. Comput.*, 19, 297-301, 1965.
- de Zutter, D., The dyadic Green's function for the Fourier spectra of the fields from harmonic sources in uniform motion, *Electromagnetics*, 2, 221-237, 1982.
- de Zutter, D., Green's function for the Fourier spectra of the fields from two-dimensional sources or scatterers in uniform motion, *Radio Sci.*, 22, 1197-1203, 1987.
- Doppler, C. J., Über das farbige Licht der Doppelsterne und einiger anderer Gestirne des Himmels, *Abh. K. Böhmischen Ges. Wiss.*, 2, 467-482, 1842.
- Enggheta, N., An overview of the theory of the near zone inverse Doppler effect, in *Recent Advances in Electromagnetic Theory*, edited by H. N. Kritikos and D. L. Jaggard, pp. 56-73, Springer-Verlag, New York, 1990.
- Enggheta, N., A. R. Mickelson, and C. H. Papas, On the near-zone inverse Doppler effect, *IEEE Trans. Antennas Propag.*, AP-28, 512-522, 1980.
- Frank, I. M., Doppler effect in a refractive medium, *J. Phys. USSR*, 2, 49-67, 1943.
- Gill, T. P., *The Doppler Effect*, Academic, San Diego, Calif., 1965.
- Ifeachor, E. C., and B. W. Jervis, *Digital Signal Processing: A Practical Approach*, Addison-Wesley, Reading, Mass., 1993.
- Kay, S. M., *Modern Spectral Estimation: Theory and Application*, Prentice Hall, Englewood Cliffs, N. J., 1988.
- Marple, S. L., Jr., *Digital Spectral Analysis with Applications*, Prentice Hall, Englewood Cliffs, N. J., 1987.
- Michielsen, B. L., G. C. Herman, A. T. de Hoop, and D. de Zutter, Three-dimensional relativistic scattering of electromagnetic object in uniform translational motion, *J. Math. Phys.*, 22, 2716-2722, 1981.
- Papas, C. H., *Theory of Electromagnetic Wave Propagation*, McGraw-Hill, New York, 1965.
- Papoulis, A., *Signal Analysis*, McGraw-Hill, New York, 1977.
- Rydbeck, D. E. H., The Doppler effect in dispersive, inhomogeneous media with applications to electromagnetic waves in ionized media, *Res. Rep. 10*, 75 pp., Res. Lab. of Electron., Chalmers Univ. of Technol., Gothenburg, Sweden, 1960.
- Stratton, J. A., *Electromagnetic Theory*, McGraw-Hill, New York, 1941.
- Vakman, D. E., *Sophisticated Signals and the Uncertainty Principle in Radar*, Springer-Verlag, New York, 1968.
- Van Bladel, J., *Electromagnetic Fields*, Hemisphere, New York, 1985.

Y. Ben-Shimol and D. Censor, Department of Electrical and Computer Engineering, Ben-Gurion University of the Negev, Box 653, Beer-Sheva, 84105, Israel. (e-mail: yehuda@eesrv.ee.bgu.ac.il; censor@eesrv.ee.bgu.ac.il)

(Received March 3, 1997; revised December 5, 1997; accepted January 5, 1998.)